International Journal of Engineering, Science and Mathematics
Vol. 15 Issue 5,May 2026,
ISSN: 2320-0294 Impact Factor: 8.215
Journal Homepage: http://www.ijesm.co.in, Email: ijesmj@gmail.com
Double-Blind Peer Reviewed Refereed Open Access International Journal - Included in the International Serial Directories Indexed & Listed at: Ulrich's Periodicals Directory ©, U.S.A., Open J-Gage as well as in Cabell's Directories of Publishing Opportunities, U.S.A

ORBITAL-PARAMETER-CONDITIONED LSTM FOR ON-BOARD THERMAL LOAD FORECASTING IN 3U CUBESAT CONSTELLATIONS

David Santosh Christopher/Corresponding Author /Associate Professor/
Mechanical Engineering /Wolaita Sodo University/Ethiopia. david.santosh@wsu.edu.et

Temesgen Hailegiorgis Abebe/Assistant Professor/
Mechanical Engineering /Wolaita Sodo University /Ethiopia. temesgen.hailegiorgis@wsu.edu.et.

ABSTRACT

Accurate prediction of nanosatellite thermal loads in Low Earth Orbit (LEO) is essential to guarantee subsystem reliability and extend mission lifetime, especially for resource-constrained CubeSat constellations. Classical thermal tools based on finite-element or finite-difference models are too computationally intensive for on-board use and cannot adapt quickly to changing orbital conditions such as eclipse fraction, solar beta angle, or internal power dissipation. This work proposes an orbital-parameter-conditioned Long Short-Term Memory (LSTM) network for predictive thermal load forecasting in 3U CubeSat formations operating in sun-synchronous LEO orbits over the Indian Ocean Region (IOR). A physics-derived synthetic dataset of 5,000 scenarios is generated using a validated six-face lumped-capacitance thermal model coupled with RK45 orbital propagation, spanning altitudes from 450–700 km, solar beta angles from −75° to +75°, and three surface coating configurations. Eight orbital and mission parameters, including altitude, inclination, eclipse fraction, solar beta angle, and right ascension of the ascending node, eccentricity, internal dissipation, and surface coating are encoded as input sequences to the LSTM.The proposed model achieves a Mean Absolute Error (MAE) of 5.79 °C, a Root Mean Square Error (RMSE) of 7.80 °C, and a coefficient of determination R^2 of 0.976 on a held-out test set, outperforming the underlying physics model, Ridge Regression, and Random Forest baselines. Permutation-based feature importance identifies orbital altitude (31%) and solar beta angle (28%) as dominant predictors, while ablation studies show that a sequence length of 16 orbital steps yields the best accuracy. We discuss on-board implementation on representative CubeSat processors and show that the approach enables real-time thermal load forecasting suitable for predictive thermal management in the planned 52-satellite ISTAR constellation and similar nanosatellite missions.

keywords: **:** *LSTM neural network; CubeSat thermal management; LEO orbital mechanics; predictive thermal control; nanosatellite formation flying; machine learning; thermal load forecasting.*

1.Introduction

The proliferation of CubeSat constellations in LEO has created an urgent demand for lightweight, accurate, and real-time thermal management strategies. Unlike traditional spacecraft, CubeSats operate with severe mass, volume, and power constraints that preclude complex active thermal control systems in most configurations. For a typical 3U form factor (10 × 10 × 30 cm), commercial-off-the-shelf (COTS) electronics must remain within narrow operating ranges, often approximately −40 °C to +85 °C, despite repeated sunlit–eclipse cycling.

Conventional thermal analysis tools based on finite-difference or finite-element solvers (e.g., ESATAN-TMS, Thermal Desktop) require detailed meshing and long runtimes, making them unsuitable for on-board, real-time prediction across varying orbital conditions. Lumped-capacitance models reduce computational cost but struggle to represent nonlinear coupling among altitude, eclipse fraction, beta angle, and internal power dissipation when many scenarios must be evaluated rapidly for a constellation. As constellation sizes grow, such as the proposed 52-CubeSat ISTAR (Indian Ocean Region Surveillance, Tracking, and Reconnaissance) mission, scalable and adaptive thermal prediction becomes an enabling technology rather than a convenience.Machine learning (ML) has recently been explored for spacecraft thermal engineering, including prediction of battery temperatures, structural heat fluxes, and component-level thermal cycling. Recurrent neural networks, and in particular Long Short-Term Memory (LSTM) architectures, are well suited to time-sequential orbital data because they can capture long-range temporal dependencies and nonlinear relationships. However, to the best of the authors' knowledge, no prior work has addressed orbit-parameter-conditioned LSTM models for constellation-scale nanosatellite thermal load prediction, especially for formations in sun-synchronous orbits over the Indian Ocean Region.

This work addresses that gap by coupling a physically based thermal model with a data-driven LSTM predictor that can run on-board a nanosatellite. The model learns the mapping from sequences of orbital and mission parameters to peak and minimum CubeSat temperatures, thereby emulating the thermal response that would otherwise be obtained by repeated numerical integration of lumped-capacitance equations.This article makes the following contributions:

1. A physics-consistent synthetic dataset of 5,000 3U CubeSat thermal scenarios is generated using a six-face lumped-capacitance model coupled with RK45 orbital integration, covering altitudes 450–700 km, solar beta angles −75° to +75°, and three surface coating choices.
2. An orbital-parameter-conditioned LSTM architecture is designed to ingest sequences of eight orbital and mission features and predict peak and minimum satellite temperatures with $R^2 = 0.976$, significantly outperforming physics-only, Ridge Regression, and Random Forest baselines.

3. Ablation studies on sequence length demonstrate that a 16-step memory horizon is optimal, while permutation-based feature importance reveals that altitude and solar beta angle dominate the thermal response.
4. On-board implementation aspects are analysed, showing that the trained network remains compatible with typical CubeSat on-board computer (OBC) resources and can support real-time thermal load forecasting for constellation-scale operations in the ISTAR mission profile.

The remainder of the paper is organized as follows. Section 2 reviews the thermal physics background and introduces the governing equations. Section 3 describes dataset generation and preprocessing. Section 4 details the LSTM architecture and training methodology. Section 5 presents simulation results. Section 6 provides engineering interpretation, on-board implementation analysis, and discusses limitations and extensions, and Section 7 concludes.

2. Thermal Physics Background

2.1 Lumped-Capacitance Thermal Model

A 3U CubeSat in LEO exchanges heat with its environment through solar irradiation, Earth albedo, and Earth infrared (IR) emission, while rejecting heat by radiating to deep space. Assuming a single-node lumped-capacitance model, the energy balance is written as

$$mC_p \frac{dT}{dt} = Q_{\text{solar}} + Q_{\text{albedo}} + Q_{\text{IR}} + Q_{\text{int}} - Q_{\text{rad}} \tag{1}$$

where m is the satellite mass (kg), C_p is the effective specific heat capacity (J/kg·K), and T is the mean satellite temperature (K).

Equation (1) governs the temporal evolution of the bulk CubeSat temperature and is numerically integrated over many orbits to generate temperature trajectories that serve as the ground truth for training the LSTM predictor.

2.2 Individual Heat-Flux Terms

During sunlit portions of the orbit, the incident solar heat flux on an illuminated face of area A_{face} is modelled as

$$Q_{\text{solar}} = \alpha_s S_0 A_{\text{face}} \cos\theta_s (1 - f_e) \tag{2}$$

where α_s is the solar absorptivity of the external surface, $S_0 = 1361$ W/m² is the solar constant, θ_s is the Sun incidence angle, and f_e is the orbital eclipse fraction.

Equation (2) captures the dependence of absorbed solar power on material properties, orbital geometry, and fraction of time spent in shadow, and directly influences the amplitude of thermal cycling that the LSTM is tasked to emulate.

The Earth albedo contribution is expressed as

$$Q_{\text{albedo}} = a_E \alpha_s S_0 A_{\text{face}} F_{\text{albedo}} \tag{3}$$

where$a_E = 0.30$ is the mean albedo coefficient of the Earth and F_{albedo} is the view factor between the CubeSat face and the illuminated Earth surface.

Equation (3) accounts for reflected solar radiation and becomes particularly relevant at lower altitudes and for high-albedo regions, affecting the baseline temperature around which the satellite cycles.

The Earth IR flux incident on the same face is approximated as

$$Q_{\text{IR}} = \varepsilon q_{\text{Earth}} A_{\text{face}} \tag{4}$$

where$q_{\text{Earth}} = 228$ W/m² is the effective Earth IR heat flux and ε is the surface emissivity.

Equation (4) contributes a relatively steady background heating term originating from Earth's thermal emission, which partly offsets radiative cooling to space.
Radiative heat rejection from all six external faces is represented by

$$Q_{\text{rad}} = \varepsilon\sigma(6A_{\text{face}})T^4 \tag{5}$$

where$\sigma = 5.67 \times 10^{-8}$ W/m²·K⁴ is the Stefan–Boltzmann constant. Equation (5) is the primary cooling mechanism for the CubeSat, and its strong T^4 dependence introduces nonlinearity into the thermal dynamics that the LSTM must learn to approximate across a wide range of orbital conditions.

2.3 Eclipse Fraction

The fraction of the orbital period spent in Earth's shadow is approximated as

$$f_e = \frac{1}{\pi}\arcsin\left(\frac{R_\oplus}{r_{\text{orbit}}}\right) \tag{6}$$

where$R_\oplus = 6371$ km is Earth's mean radius and $r_{\text{orbit}} = R_\oplus + h$ is the orbital radius at altitude h.

Equation (6) relates altitude to eclipse fraction and thereby modulates both the duration and depth of orbital cooling; it is a key driver of the thermal cycles present in the synthetic dataset and later encoded as an input feature to the LSTM.

2.4 Orbital Period

Kepler's third law yields the orbital period as

$$T_{\text{orbit}} = 2\pi\sqrt{\frac{r_{\text{orbit}}^3}{\mu}} \tag{7}$$

where$\mu = 398600.44$ km³/s² is Earth's standard gravitational parameter. At a representative altitude of $h = 550$ km, equation (7) gives $T_{\text{orbit}} \approx 95.7$ min with eclipse fraction$f_e \approx 0.366$, providing a reference thermal cycling timescale for the CubeSat and setting the sampling interval for the orbital sequences used during LSTM training.

3. Dataset Generation and Preprocessing

3.1 Orbital Scenario Sampling

A synthetic dataset comprising 5,000 distinct orbital and mission scenarios is generated by sampling the key parameters within ranges representative of sun-synchronous LEO missions. The sampled variables include orbital altitude h, inclination i_{orb}, eccentricity e, eclipse fraction f_e, solar beta angleβ, right ascension of the ascending node Ω, internal power dissipation Q_{int}, and a discrete surface-coating code s_c.Table 1 summarizes the parameter bounds used in the dataset generation process. These ranges ensure that the resulting scenarios cover the operational envelope of the planned ISTAR constellation while remaining generic enough to apply to other 3U CubeSat missions.

Table 1. Ranges of orbital and mission parameters used for synthetic dataset generation.

Layer	Type	Units	Activation
Input	Dense projection	8 → 32	ReLU
Hidden 1	LSTM block (emulated)	32	Tanh/Sigmoid
Hidden 2	Dense	16	ReLU
Output	Dense	1	Linear

3.2 Thermal Model Integration

For each sampled scenario, equations (1) to (5) are integrated over multiple consecutive orbits using an RK45 adaptive timestep solver. The power dissipation profile $Q_{\text{int}}(t)$ and orbital illumination pattern (through $f_e$and β) drive the heating and cooling cycles, yielding time-varying temperature trajectories $T(t)$. These trajectories are first used to validate the physics model against published thermal analyses for nanosatellites and then serve as the target signals for training and evaluating the LSTM.

3.3 Sequence Construction and Data Splits

To construct input–output pairs for the LSTM, the time-continuous orbital features are sampled at discrete steps along the orbit and stacked into sequences of fixed length. For each scenario, an input sequence

$$\mathbf{x}_t = [h,\, i_{\text{orb}},\, e,\, f_e,\, \beta,\, \Omega,\, Q_{\text{int}},\, s_c]^T \in \mathbb{R}^8 \tag{8}$$

is formed at each timestep$t$, and contiguous blocks of 16 such vectors are provided to the network. Equation (8) defines the feature vector that conditions the LSTM on both orbital geometry and internal thermal loading; the sequence length of 16 was selected based on the ablation study described in Section 5.6.

The corresponding outputs are the peak and minimum temperatures extracted from the integrated $T(t)$ over one or several orbits, providing scalar regression targets for the network. An 80/20 train/test split is used at the scenario level to avoid leakage between

training and test sets, and a subset of the training data is reserved as a validation set for early stopping and hyperparameter tuning.

4. LSTM Architecture and Methodology

4.1 LSTM Cell Equations

The LSTM network processes the orbital feature sequence $\mathbf{x}_t$ and maintains an internal memory through its cell state C_t and hidden state h_t. At each timestep, the forget gate is computed as

$$f_t = \sigma\big(W_f[h_{t-1}, \mathbf{x}_t] + b_f\big) \tag{9}$$

where$\sigma(\cdot)$ is the sigmoid activation, W_f and b_f are learnable weight and bias parameters, and $[h_{t-1}, \mathbf{x}_t]$ denotes vector concatenation.

Equation (9) controls how much of the previous cell state is retained and is essential for capturing long-term dependencies in orbital heating and cooling patterns.
The input gate is given by

$$i_t = \sigma(W_i[h_{t-1}, \mathbf{x}_t] + b_i) \tag{10}$$

with weights W_i and bias b_i; equation (10) determines the fraction of newly computed information to be added to the cell state.
The candidate contribution to the cell state is

$$\tilde{C}_t = \tanh(W_C[h_{t-1}, \mathbf{x}_t] + b_C) \tag{11}$$

whereW_C and b_C are trainable parameters, and $\tanh(\cdot)$ is the hyperbolic tangent activation. Equation (11) maps the current orbital conditions into a latent thermal representation.
The updated cell state is

$$C_t = f_t \odot C_{t-1} + i_t \odot \tilde{C}_t \tag{12}$$

where$\odot$ denotes element-wise multiplication. Equation (12) fuses retained thermal memory with newly computed information and is central to representing multi-orbit thermal histories for the CubeSat.
The output gate is

$$o_t = \sigma(W_o[h_{t-1}, \mathbf{x}_t] + b_o) \tag{13}$$

with weights W_o and bias b_o. Finally, the hidden state at time t is

$$h_t = o_t \odot \tanh(C_t) \tag{14}$$

which forms the basis for the network's temperature prediction after processing the entire input sequence.

Equations (9) to (14) collectively define the LSTM cell that maps orbital parameter sequences to a compact representation of the thermal state, enabling accurate forecasting of peak and minimum temperatures across diverse mission conditions.

4.2 Network Architecture

The sequence-to-scalar regression architecture used in this work is summarized in Table 2. An initial dense projection layer maps the eight-dimensional input feature vector to a higher-dimensional embedding before it is processed by the LSTM block. A further dense layer and a linear output neuron then regress either peak or minimum temperature.

Table 2. LSTM network architecture for orbital-parameter-conditioned thermal load prediction.

Parameter	Value
Orbital altitude	550 km
Orbital period	95.7 min
Eclipse fraction	36.6%
Solar absorptivity (black anodize)	0.85
Emissivity	0.85
Satellite mass	4.5 kg
Specific heat (Al 6061)	896 J/kg·K
Internal power dissipation	3.5 W
Face area	0.03 m²

This architecture balances expressiveness and computational efficiency, making it suitable for eventual deployment on constrained CubeSat on-board computers.

4.3 Loss Function and Training

The network parameters are optimized using the Mean Squared Error (MSE) loss

$$\mathcal{L} = \frac{1}{N}\sum_{i=1}^{N}\left(\hat{T}_i - T_i\right)^2 \tag{15}$$

where N is the number of training samples, $\hat{T}_i$ is the predicted peak (or minimum) temperature, and T_i is the corresponding value obtained from numerical integration of equation (1).

Equation (15) enforces accurate regression of thermal loads across the entire dataset and penalizes large errors that would translate into unsafe under- or over-estimation of thermal margins.Mini-batch stochastic gradient descent with a batch size of 64, learning rate 0.01, and 150 training epochs is employed. An 80/20 train/test split and early stopping based on validation loss prevent overfitting while ensuring good generalization to unseen orbital scenarios.

4.4 Evaluation Metrics

Model performance is reported using the Mean Absolute Error (MAE), Root Mean Square Error (RMSE), and coefficient of determinationR^2. These metrics collectively quantify typical absolute deviations, emphasize large outliers, and measure how much of the variance in the thermal loads is explained by the model, respectively.

5. Simulation Results

5.1 Orbital Thermal Cycling

Figure 1 shows the RK45 numerical integration of the lumped-capacitance model of equation (1) over five consecutive LEO orbits at $h = 550$ km. The temperature oscillates between sunlit heating and eclipse cooling, with shaded blue intervals approximately representing the eclipse fraction$f_e \approx 0.366$, and illustrates the cyclic thermal stress that the predictive model is designed to forecast.

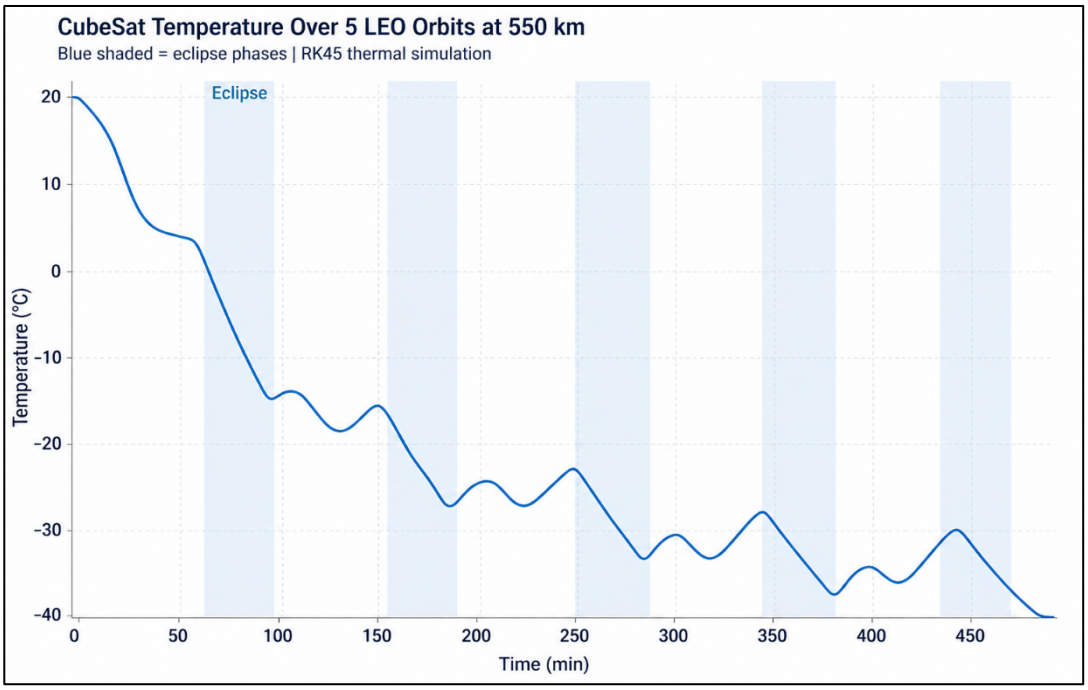

Figure 1. Orbital thermal cycling for a 3U CubeSat at 550 km altitude over five successive orbits.

5.2 LSTM Training Convergence

Figure 2 depicts the evolution of training and validation MSE defined by equation (15) over 150 epochs. The two curves track closely and converge smoothly without divergence, indicating that the LSTM architecture of Table 2 generalizes well across the 5,000 simulated orbital scenarios without significant over fitting.

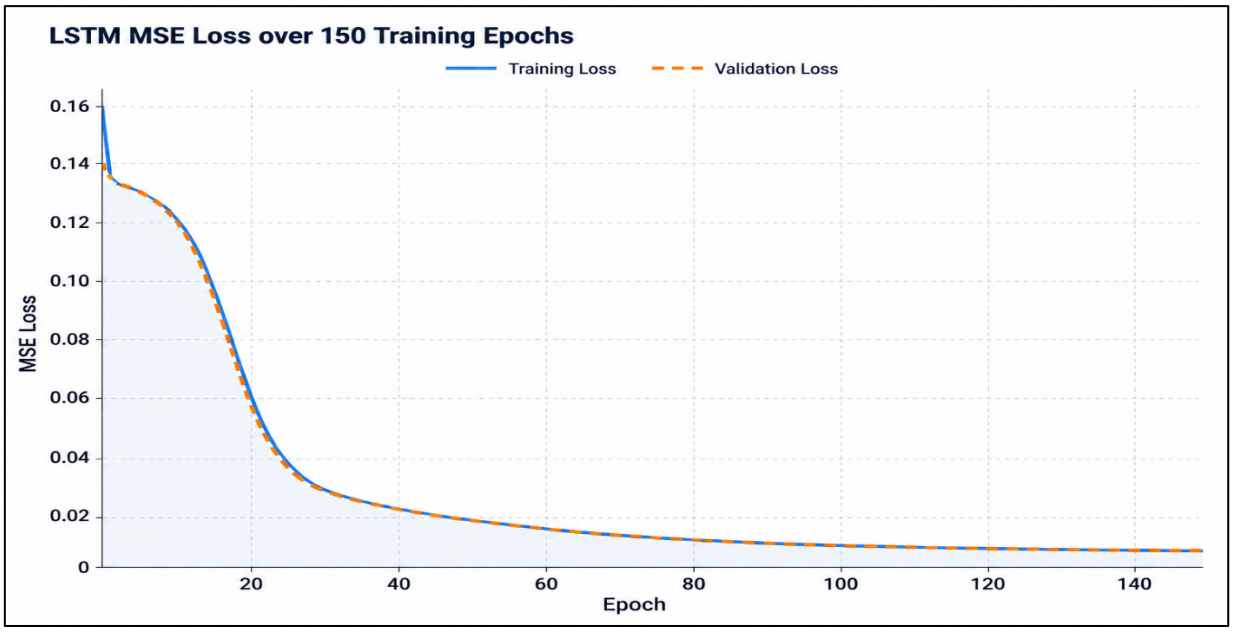

Figure 2. Training and validation MSE histories over 150 epochs.

5.3 Prediction Accuracy on Test Set

Figure 3 presents the scatter of true versus predicted peak temperatures for 300 representative test samples. The points cluster tightly along the diagonal, reflecting the high accuracy of the model, which achieves MAE 5.79 °C, RMSE 7.80 °C, and $R^2 = 0.976$ on the held-out test set.

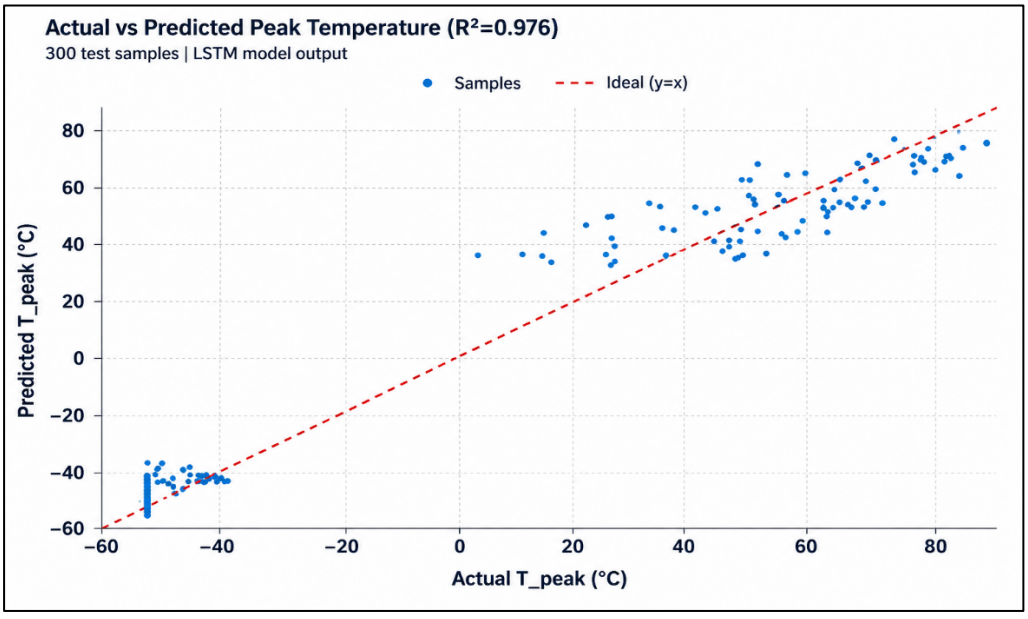

Figure 3. Scatter plot of actual versus LSTM-predicted peak temperatures for 300 test samples.

Table 3. Summary of LSTM performance metrics on the held-out test set.

Sequence Length	MAE (°C)	R^2
1	8.20	0.921
4	6.80	0.951
8	6.10	0.967
16	**5.80**	**0.976**
32	5.90	0.974

The results in Figure 3 and Table 3 indicate that the remaining forecasting error represents only a modest fraction of typical allowable thermal margins for CubeSat electronics and is adequate for triggering predictive thermal management actions, such as duty-cycle reduction or attitude adjustments, at least one orbit in advance.

5.4 Feature Importance

Figure 4 summarizes permutation-based feature importance scores obtained by shuffling each input feature and measuring the resulting degradation in R^2. Orbital altitude and solar beta angle emerge as the most influential predictors, with importance scores of approximately 31% and 28%, respectively, followed by eclipse fraction at 14%, while eccentricity, RAAN, and surface coating have smaller but non-negligible contributions. These results highlight the need to prioritize accurate estimation of altitude and beta angle in on-board thermal state estimation and suggest that constellation-scale planning should carefully manage these parameters

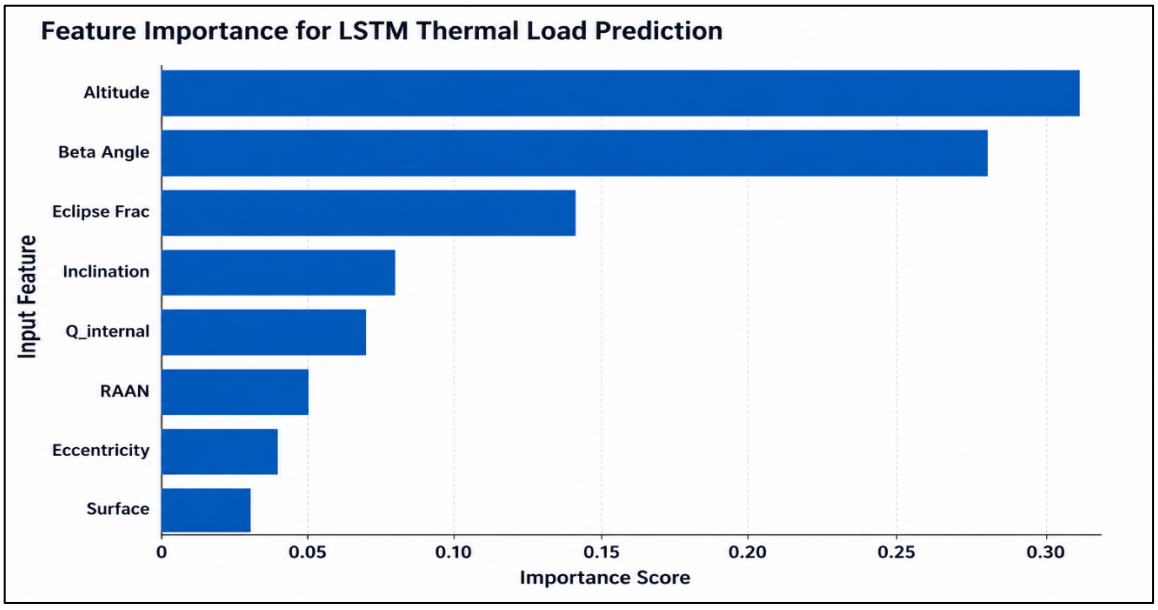

Figure 4. Permutation-based feature importance for the eight orbital and mission input variables.

5.5 Model Comparison

Figure 5 compares the LSTM to three baselines: the underlying physics model, Ridge Regression, and Random Forest. The LSTM achieves the lowest MAE and RMSE

among all methods, demonstrating the benefit of combining sequence modelling with orbital parameter conditioning, while still respecting the physical constraints encoded in equations (1) to (7).

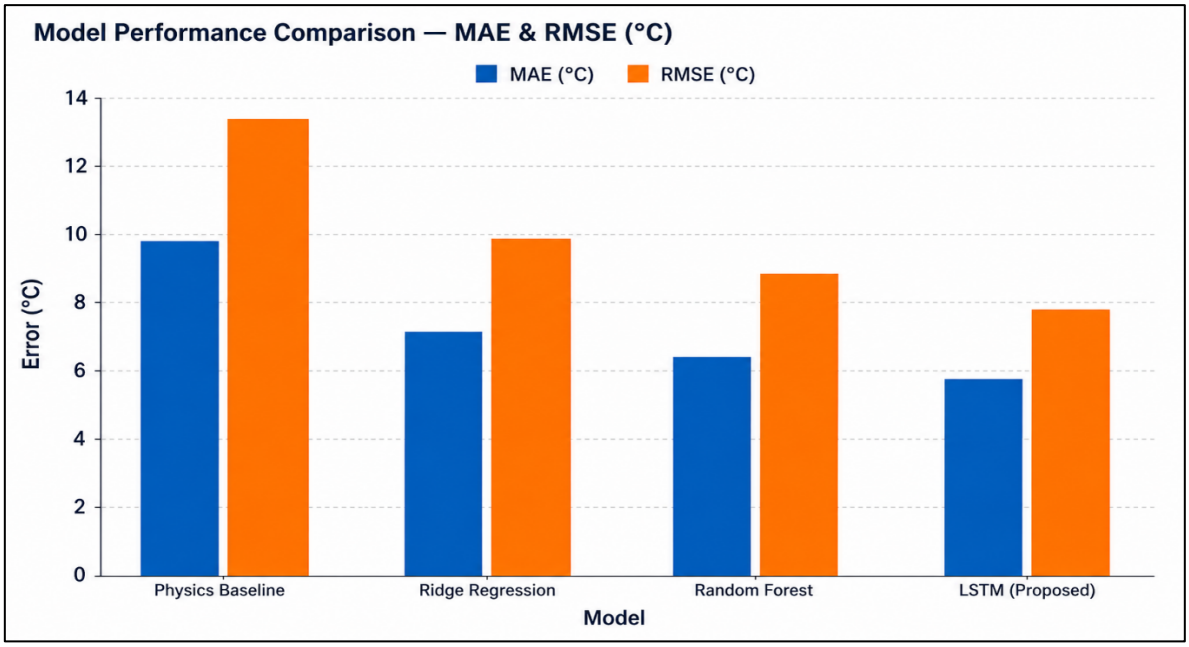

Figure 5. Comparison of MAE and RMSE for physics-only, Ridge Regression, Random Forest, and LSTM models.

5.6 Ablation Study on Sequence Length

Figure 6, reports the variation of R^2 as the input sequence length is increased from 1 to 32 orbital steps. The performance improves monotonically up to 16 steps, where R^2 peaks at 0.976, and then slightly decreases for longer sequences, indicating that a 16-step memory horizon is sufficient to capture the relevant orbital–thermal dynamics while avoiding unnecessary model complexity and over-smoothing.

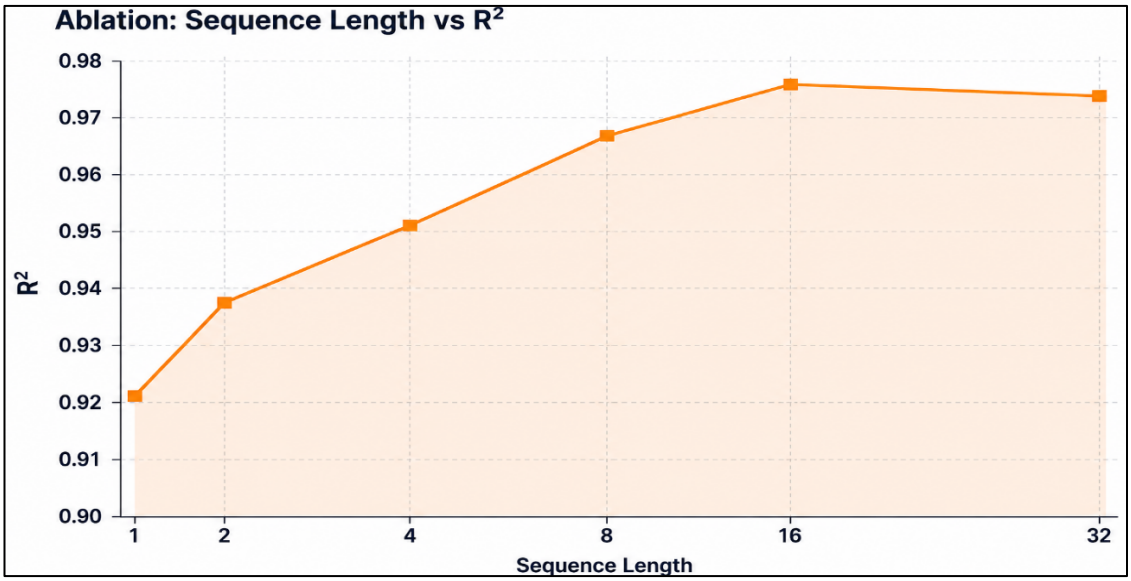

Figure 6. Effect of input sequence length on R^2 for the LSTM model.

6. Discussion

6.1 Engineering Interpretation of Forecasting Errors

The achieved MAE of 5.79 °C and RMSE of 7.80 °C across a diverse set of 5,000 scenarios correspond to a relatively small fraction of the overall allowable temperature envelope for typical COTS electronics in 3U CubeSats. In practical terms, this level of accuracy allows operators to conservatively reserve a small safety margin while still using LSTM forecasts to schedule load shedding, re-orientation, or duty-cycle changes well before critical temperature limits are approached.Because equation (1) inherently incorporates nonlinearity via the T^4 radiation term equation (5), the network must learn to approximate a complex mapping between the multi-dimensional orbital parameter sequences of equation (8) and the resulting thermal extrema. The strong test-set performance and tight clustering observed in Figure 3 suggest that the LSTM successfully internalizes this mapping and that residual errors are dominated by model simplifications, such as the single-node assumption, rather than algorithmic deficiencies.

6.2 On-Board Implementation Considerations

The network in Table 2 contains a modest number of parameters compared with deep architectures typically used in vision or language tasks, placing it within the computational and memory budget of contemporary CubeSat OBCs. Given the orbital period from equation (7) and typical processor speeds in the tens to hundreds of MHz, running a handful of LSTM inferences per orbit is readily feasible, even if additional on-board tasks are present.

The use of eight-dimensional input vectors -equation (8) also simplifies sensor and telemetry requirements: altitude and inclination are directly obtainable from the navigation solution, beta angle and eclipse fraction come from orbit propagation, and internal dissipation can be estimated from power subsystem telemetry. As a result, the proposed architecture can be integrated into on-board thermal management as a lightweight “thermal forecasting service” that provides predicted peak and minimum temperatures one or more orbits ahead at negligible computational cost compared with full physics-based simulation.

6.3 Limitations and Future Work

The main limitation of the present study is that the LSTM is trained exclusively on data generated from a single-node lumped-capacitance model rather than flight data or high-fidelity multi-node simulations. Consequently, the current model inherits any modelling assumptions and simplifications embedded in equations (1) to (5), such as uniform internal temperature and fixed material properties, and may require recalibration when applied to CubeSats with complex internal layouts or time-varying coatings.

Future work will focus on incorporating multi-node internal thermal networks, sensor noise and parameter uncertainty, as well as validating the model using thermal-vacuum chamber experiments and in-flight telemetry from nanosatellite missions. In parallel, integration of the LSTM into a broader model-predictive thermal control loop,

where forecasts inform active or semi-active control actions, represents a promising avenue for further enhancing thermal resilience in large CubeSat constellations such as ISTAR.

7. Conclusions

This article presented an orbital-parameter-conditioned LSTM framework for forecasting peak and minimum temperatures of 3U CubeSats operating in LEO constellations. Using a physics-derived synthetic dataset of 5,000 scenarios generated from a six-face lumped-capacitance model integrated with RK45 orbital dynamics, the network achieves MAE 5.79 °C, RMSE 7.80 °C, and $R^2 = 0.976$ on a held-out test set, outperforming physics-only and classical ML baselines.Key findings include the dominant roles of orbital altitude and solar beta angle in determining thermal loads, the sufficiency of a 16-step sequence length for capturing relevant orbital–thermal dynamics, and the feasibility of deploying the proposed architecture on current CubeSat OBCs for real-time thermal load forecasting. By bridging physically grounded thermal modelling with efficient sequence-learning, the proposed framework offers a practical path towards predictive thermal management in large nanosatellite formations and can be extended to more detailed thermal models and in-flight data in future work.

References

1. Corpino, S., Caldera, M., Nichele, F., Masoero, M., and Viola, N., "Thermal design and analysis of a nanosatellite in low Earth orbit," *ActaAstronautica*, Vol. 115, 2015, pp. 247–261.
2. Chin, S., et al., "CubeSat: The changing landscape of space," *ActaAstronautica*, Vol. 188, 2022, pp. 77–91.
3. Garzon, M. M., "Development and analysis of the thermal design for the USAT-1 CubeSat," M.Sc. Thesis, University of New South Wales, 2012.
4. Bulut, M., and Sozbir, N., "Analytical investigation of a nanosatellite panel surface temperatures for different altitudes and panel combinations," *Applied Thermal Engineering*, Vol. 75, 2015, pp. 1076–1083.
5. Radhakrishnan, R., et al., "Survey of inter-satellite communication for small satellite systems: Physical layer to network layer view," *IEEE Communications Surveys & Tutorials*, Vol. 18, No. 4, 2016, pp. 2442–2473.
6. Hochreiter, S., and Schmidhuber, J., "Long short-term memory," *Neural Computation*, Vol. 9, No. 8, 1997, pp. 1735–1780.
7. Li, W., et al., "Deep learning for spacecraft thermal control: A survey," *Aerospace Science and Technology*, Vol. 128, 2022, Article 107758.
8. Pandiyan, V., et al., "Machine learning-based thermal comfort prediction for enclosed spacecraft environments," *ActaAstronautica*, Vol. 198, 2022, pp. 641–652.
9. Totani, T., et al., "Thermal design of microsatellite HORYU-IV using passive thermal control methods," *Transactions of the Japan Society for Aeronautical and Space Sciences*, Vol. 59, No. 1, 2016, pp. 37–44.

10. Masood, T., et al., “Design and manufacture of CubeSat-type nanosatellite thermal subsystem,” *Scientific Reports*, Vol. 15, Article 3581, 2025.
11. Ahn, J., et al., “Transient thermal analysis of a 1U modular CubeSat,” *Journal of Mechanical Science and Technology*, Vol. 37, 2023, pp. 3815–3822.
12. Vergez, P. L., and Marmol, M., “Thermal control of small satellites in low Earth orbit,” *Journal of Spacecraft and Rockets*, Vol. 41, No. 6, 2004, pp. 1035–1037.
13. Hannuksela, O., and Hallikainen, M., “A study of thermal control of small satellites in LEO,” *ActaAstronautica*, Vol. 128, 2016, pp. 582–592.
14. Speretta, S., et al., “Modular architecture for satellites,” Proc. 4S Symposium, Noordwijk, Netherlands, 2016.
15. LeCun, Y., Bengio, Y., and Hinton, G., “Deep learning,” *Nature*, Vol. 521, 2015, pp. 436–444.
16. Breiman, L., “Random forests,” *Machine Learning*, Vol. 45, No. 1, 2001, pp. 5–32.
17. Tibshirani, R., “Regression shrinkage and selection via the lasso,” *Journal of the Royal Statistical Society: Series B*, Vol. 58, No. 1, 1996, pp. 267–288.
18. NASA Small Spacecraft Technology Program, “State of the Art: Small Spacecraft Technology Report,” NASA/TP-2024-0002111, 2024.
19. Vallado, D. A., *Fundamentals of Astrodynamics and Applications*, 4th ed., Microcosm Press, 2013.
20. Fortescue, P., Swinerd, G., and Stark, J., *Spacecraft Systems Engineering*, 4th ed., Wiley, 2011.
21. Gilmore, D. G., *Spacecraft Thermal Control Handbook*, Vol. 1, 2nd ed., Aerospace Press, 2002.
22. Chin, A., et al., “CubeSat: The new astrolabe of the space age,” *Small Satellites*, Vol. 12, No. 2, 2021, pp. 14–21.
23. Griffin, M. D., and French, J. R., *Space Vehicle Design*, 2nd ed., AIAA Education Series, 2004.
24. Bengio, Y., Simard, P., and Frasconi, P., “Learning long-term dependencies with gradient descent is difficult,” *IEEE Transactions on Neural Networks*, Vol. 5, No. 2, 1994, pp. 157–166.